



# Swift, versatile and a rigorous kinetic model based artificial neural network surrogate for single and multicomponent batch adsorption processes

Akhil Gopinath, Bharathi Ganesan Retnam, Arun Muthukkumaran, Kannan Aravamudan \*

Department of Chemical Engineering, Indian Institute of Technology Madras, Chennai, 600036, India

## ARTICLE INFO

### Article history:

Received 29 May 2019

Received in revised form 30 September 2019

Accepted 7 October 2019

Available online 23 October 2019

### Keywords:

Adsorption kinetics

Multicomponent adsorption

Homogeneous surface diffusion model (HSDM)

Artificial neural network (ANN)

Computational efficiency

## ABSTRACT

Rigorous and robust first principles-based Homogeneous Surface Diffusion Model (HSDM) is demonstrated for numerical simulation and estimation of surface diffusivities for single, binary and ternary systems involving dyes and pharmaceutical molecules. The current work's novelty lies in proposing a fast, reliable and efficient Artificial Neural Network (ANN) surrogate to the mechanistic HSDM. Repeated numerical integration of the model's partial differential equations during parameter estimation from batch adsorption kinetics data is highly time-consuming and is not required for the proposed approach. This ANN was trained by a small number of HSDM simulations and limited experimental batch kinetics data with different combinations of surface diffusivity ( $D_s$ ) values. ANNs were developed and tested against the experimentally obtained batch kinetics data for various systems. The trained ANN was able to capture the kinetics that was rigorously predicted using HSDM. A 99.9%, 98.6% and 99.3% similarity could be achieved between  $D_s$  values estimated using HSDM and ANN for single, binary and ternary systems respectively. Similarly, the batch kinetics data was almost identically tracked by ANN. The computational time required for this novel ANN per simulation reduced spectacularly and was about 14 times lesser while the total parameter estimation time was about 17 times lesser than HSDM. The ANN developed for estimating parameters could be operated in reverse as well for simulating the multicomponent batch adsorption kinetics and tracking the increase in percentage removal of the solutes with time at different process conditions. Irrespective of number of components, the ANNs performances were consistent. The ratio of neurons and their total number in the hidden layers had a significant impact on the performance. Hence optimization of network parameters is essential to realize the benefits of ANN. The shortcomings of empirical kinetic models viz. Pseudo First Order model (PFO) and Pseudo Second Order model (PSO) were also demonstrated. This work demonstrates the utility of ANNs in rigorous multicomponent adsorption kinetics applications and has considerable potential in real time optimization and operation of wastewater treatment plants.

© 2019 Elsevier B.V. All rights reserved.

## 1. Introduction

Dye contaminated water discharge into water bodies by various industries is one of the major contributors to water pollution. Dye molecules are not only harmful to humans but the entire ecosystem [1]. Dye concentration of as low as 0.1 mg/L in water makes it undrinkable [2]. Another class of emerging contaminants is Pharmaceutically Active Compounds (PhAC) whose presence in water bodies is subject to extensive research in recent times [3–7].

Adsorption is the most employed technique in removal of these compounds owing to its ease of operation, ability to remove even low levels of pollutants and absence of any hazardous by-product [8–11]. Adsorption is a complex interfacial phenomenon and has applications in technological, biological and environmental processes viz wastewater treatment, catalysis, bio-implants, cooling systems to name few [12–19]. Adsorption systems are relatively easy and inexpensive to operate [20].

The percentage removal of solutes from the fluid is the primary parameter in adsorption processes as it determines the design of the associated separation units. Percentage removal is related to the main input parameters such as initial concentration ( $C_0$ ), pH, temperature (T) and adsorbent type, in a highly sophisticated manner. The evolution of percentage removal with time is indicative of transportation rates and represents the kinetics of the adsorption

\* Corresponding author.

E-mail address: [kannan@iitm.ac.in](mailto:kannan@iitm.ac.in) (K. Aravamudan).

system. It is critical to know the kinetics of adsorption at various input conditions to design and operate the system at optimum conditions. While isotherms signify the capacity of the treatment, it is the kinetics that determines the size and/operating time of the adsorption unit. The kinetic data or the associated parameters are not available at many of the process conditions due to expensive experimental testing and time requirements [21]. In such situations, kinetic models may serve as useful predictive tools and different approaches have been adopted to fit kinetic data and later use them in process simulation, prediction and optimization [22,23].

Pseudo First Order model (PFO) and Pseudo Second Order model (PSO) (equations (1) and (2)) are extensively used empirical adsorption kinetic models in adsorption [24–31]. These have also been used in multicomponent systems [32–34].

$$q(t) = q_e (1 - e^{-k_1 t}) \quad (1)$$

$$q(t) = q_e^2 \frac{k_2 t}{1 + k_2 q_e t} \quad (2)$$

These empirical models do not explicitly reflect the kinetic and equilibrium mechanisms involved in the bulk fluid phase, interface and within the adsorbent. Plazinski et al. [35] observed that the simple expression given by the PFO does not distinguish between the diffusional resistance and the resistance to adsorption/desorption on active sites. Any theoretical interpretations made from PFO and PSO are specific to the chosen system and applicable only for a narrow range of operating conditions. Recently Guo and Wang [36] observed that the specific theoretical meanings and application conditions of the PFO and PSO models have not been systematically evaluated. Hence they developed a mixed order kinetic model for describing the adsorption at any stage and at any arbitrary initial solute concentration.

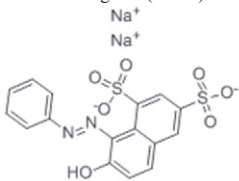
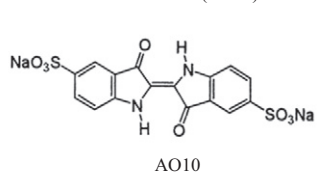
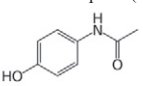
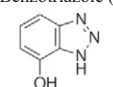
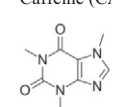
The mechanistic Homogeneous Surface Diffusion Model (HSDM) accounts for bulk convection in the fluid phase and surface diffusion through the interior of the adsorbent, with equilibrium prevailing at

the interface [19]. Hence, HSDM is more rigorous in describing adsorption kinetics [19,37]. However, HSDM is complex relative to the empirical models and has to be solved numerically owing to the nonlinear nature of the adsorption equilibria, coupled partial differential equations and the possibility of an integro-partial differential equation as a boundary condition. These generally preclude an analytical solution. Further, the governing partial differential equations are stiff and very fine resolution of space and time are required to solve them accurately. Hence, solving HSDM numerically is computationally taxing.

When, the external mass transfer resistance in the bulk fluid phase is minimized by sufficient mechanical agitation, HSDM requires only the estimate of surface diffusion coefficient ( $D_s$ ) parameter in order to solve the model equations and generate the composition profiles of the solute in the fluid and solid phases [19,37].  $D_s$  estimates are usually unavailable owing to the uniqueness of the adsorbent and the system under study. Hence, they need to be found by fitting the HSDM to the batch kinetics experimental data.

Computational intelligence models are more adaptable and efficient for complex systems with nonlinearities or insufficient data [38]. Artificial Neural Network (ANN) is a computational intelligence model inspired by the biological nervous system [38]. ANN may directly learn from experimental data without enforcing any assumptions on the data for modelling [21]. A comprehensive review on applications of ANN has been given by Ghaedi and Vafaei [21] and also by Madan et al. [39], which shows that ANN has been extensively used in modelling adsorption systems. The majority of work on ANN for adsorption system concerns with percentage removal and/or equilibrium isotherm modelling [39–47]. These are both related to the equilibrium loading on the adsorbent under different conditions. There have been limited studies on modelling adsorption kinetics using ANN trained by pseudo second-order kinetic models [48]. The present work examines the kinetics modelling of single, binary and ternary component systems through different approaches. It elaborates on the shortcomings of PFO and PSO. We demonstrate how ANNs may also be gainfully implemented to shed physical

**Table 1**  
Batch adsorption system details.

Parameter	Single	Binary	Ternary
Adsorptive	Acid Orange 10 (AO10) 	Acid Blue 74 (AB74) 	Acetaminophen (ACT)  Benzotriazole (BTA)  Caffeine (CAF) 
Adsorbent	Activated Carbon (AC-I)	AC-I	AC-II Acid Modified AC (MAC-II)
T (°C)	25 35	35	27 44
pH	4 8	4 8	3 7
$m_A/V_L$ (g/L)	0.8 1.6	0.8 1.6	2 1

insight into adsorption processes, rather than function solely as a black box model, relating a particular set of inputs to outputs. In this context, a system of artificial neural networks trained using HSDM model is proposed as a replacement for the rigorous albeit computationally expensive HSDM.

ANNs capturing the kinetic trends with fidelity and also estimating physically significant parameters for different operating conditions will be highly useful at different process conditions. The trained ANN may subsequently be used to obtain  $D_s$  values with new kinetic data without taking recourse to the HSDM model equations. Using ANN, the dramatic reduction in time and efforts required without compromising on the estimation and prediction accuracies are highlighted. Also, the ANN operating in a reverse direction will be able to predict the kinetics based on known/estimated  $D_s$  values almost instantaneously.

## 2. Materials and methods

### 2.1. Experimental details

Experimental equilibrium and kinetics data for single, binary and ternary component batch adsorption process using activated carbon were obtained from in-house

experiments [8,49]. The details of the single, binary and ternary systems along with the chemical structure of the solutes are given in Table 1.

In the study involving single component and binary mixtures, the same type of carbon (labelled as AC-I) procured from Active Char Products Pvt. Ltd., Edyar, Kerala was used [49]. The concentrations of the acid orange and acid blue dye solutions were measured using Jasco V-730 spectrophotometer at 477.5 nm and 610 nm. For analyses of the binary mixture of dyes, the method provided by Ewing was adopted [50]. In the study with the ternary system, activated carbon (labelled as AC-II) was sourced from Indo Carbon Ltd., Cochin. AC-II was further acid treated to give the modified activated carbon (MAC-II). The isocratic HPLC procedure utilized by Mirzajani and Kardani [51] was applied to detect the three compounds simultaneously using Jasco 230 system. The solutes were observed at 260 nm using photodiode array detector after being separated by HQsil C18 column of KyaTech (Japan). The mobile phase used was 0.01 M  $\text{KH}_2\text{PO}_4$  at pH 3 with acetonitrile in 80:20 v/v ratio at 0.8 mL/min.

The Freundlich adsorption isotherm model, equation (3), best fitted the single component equilibrium data (for acid orange 10 dye). Both the binary and ternary systems were fitted with the extended Sips isotherm, equation (4).

$$q_e = k_f C_e^{n_f} \quad (3)$$

$$q_{e,i} = \frac{Q_{m,i} C_{e,i}^{b_{s,i}}}{1 + \sum_{j=1}^3 k_{s,j} C_{e,j}^{b_{s,j}}} \quad (4)$$

The parameters required for the isotherms for various conditions given in Table 1 were found by fitting the different models to experimental equilibrium data. The isotherm

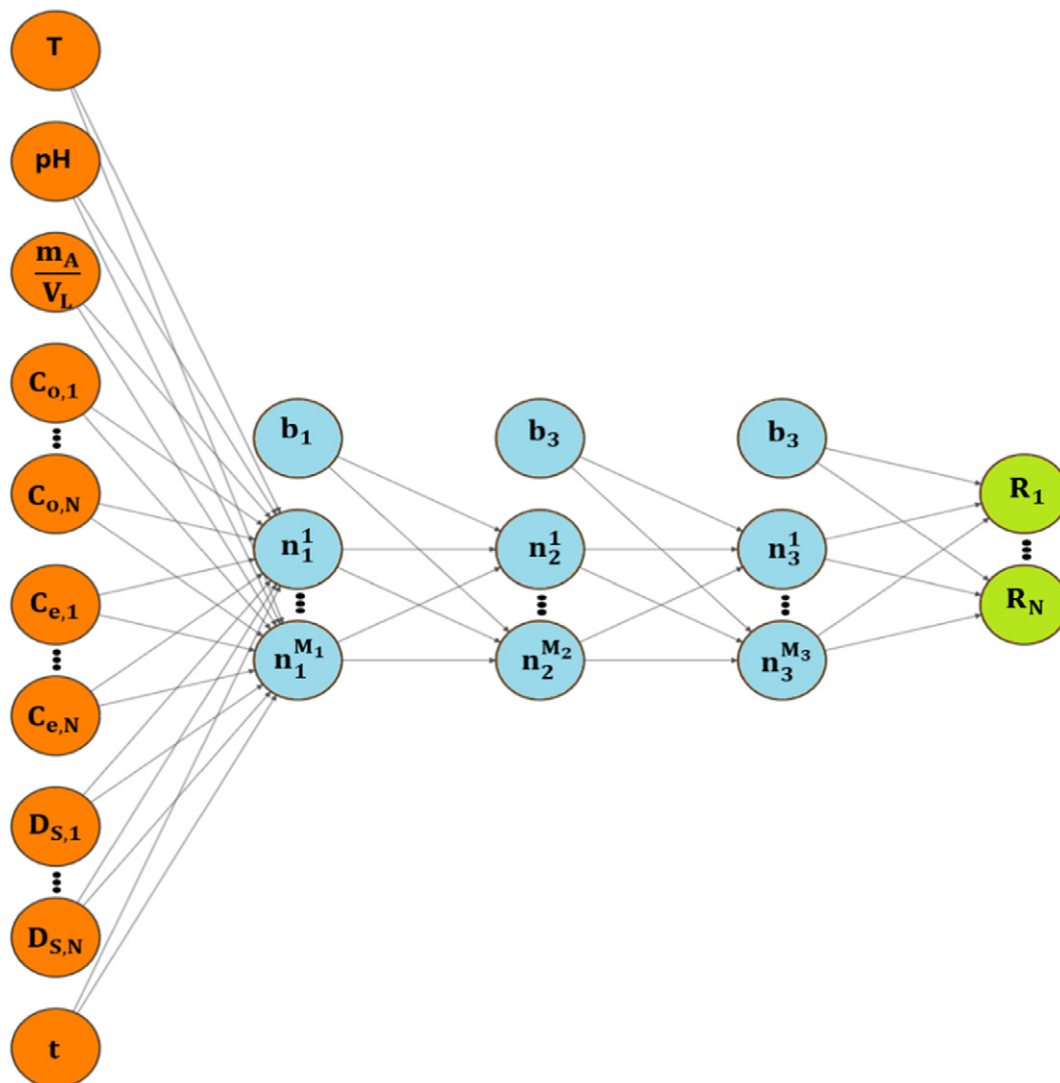


Fig. 1. ANN architecture with 3 hidden layers, each  $i$ th layer having different number of neurons ( $M_i$ ), for an  $N$ -component batch adsorption system.  $n_j^i$  and  $b_i$  correspond to  $j$ th neuron and bias in  $i$ th hidden layer respectively.

**Table 2**  
Experimental conditions used for testing the ANN.

Single Component					
Run	Activated Carbon	T (°C)	pH	$m_A/V_L$ (g/L)	$C_o$ (mg/L)
1	AC-I	25	4	0.8	300
2	AC-I	25	4	0.8	100
3	AC-I	25	4	1.6	300
4	AC-I	25	4	1.6	100
5	AC-I	25	8	0.8	300
6	AC-I	25	8	0.8	100
7	AC-I	25	8	1.6	300
8	AC-I	25	8	1.6	100
9	AC-I	45	4	0.8	300
10	AC-I	45	4	0.8	100
11	AC-I	45	4	1.6	300
12	AC-I	45	4	1.6	100
13	AC-I	45	8	0.8	300
14	AC-I	45	8	0.8	100
15	AC-I	45	8	1.6	300
16	AC-I	45	8	1.6	100

Binary Components					
Run		T (°C)	pH	$m_A/V_L$ (g/L)	$C_o$ (mg/L)
1	AC-I	35	4	1.6	50, 50
2	AC-I	35	4	1.6	150, 150
3	AC-I	35	6	1.6	100,100
4	AC-I	35	8	1.6	50, 50
5	AC-I	35	8	1.6	150, 150

Ternary Components					
Run		T (°C)	pH	$m_A/V_L$ (g/L)	$C_o$ (mg/L)
1	AC-II	27	3	2	
2	AC-II	27	7	2	100,100,100
3	AC-II	44	3	2	100,100,100
4	AC-II	44	7	2	100,100,100
5	MAC-II	27	3	2	100,100,100
6	MAC-II	27	7	2	100,100,100
7	MAC-II	44	3	2	100,100,100
8	MAC-II	44	7	2	100,100,100

models were coded in MATLAB® 2019a as a function. The Sum of Square of Errors (SSE) as given in equation (5), was minimized using Particle Swarm Optimization Algorithm hybridized with *fmincon*, available inbuilt in MATLAB.

$$SSE = \sum_i (q_{i,Exp} - q_{i,Fit})^2 \quad (5)$$

## 2.2. Homogeneous surface diffusion model (HSDM)

The HSDM for describing the adsorption kinetics of an N solute system on a spherical adsorbent particle is given by Equation (6).

$$\frac{\partial q_i}{\partial t} = \frac{1}{r^2} \frac{\partial}{\partial r} \left( r^2 D_{s,i} \frac{\partial q_i}{\partial r} \right) \quad (6)$$

Equation (6) corresponds to the accumulation of ith species transported radially within the adsorbent by surface diffusion. Equation (6) needs to be redefined for the limiting condition at  $r = 0$  by using L'Hospital rule which yields

$$\frac{\partial q_i}{\partial t} = 3D_{s,i} \frac{\partial^2 q_i}{\partial r^2} \Big|_{r=0} \quad (7)$$

The resistance to mass transfer in liquid phase is negligible due to the high rate of mechanical agitation (400 RPM) and hence, the usual boundary condition involving the convective mass transfer coefficient is absent. Instead, equation (6) is coupled with the rate of decrease of solute concentration in bulk fluid based on instantaneous mass balance and is given by

$$\frac{\partial C_i}{\partial t} = -\frac{3m_A}{R_p V_L} D_{s,i} \frac{\partial q_i}{\partial r} \Big|_{r=R_p}, \quad \forall i \in [1, N] \quad (8)$$

The boundary conditions for equation (6) are given by:

$$\frac{\partial q_i}{\partial r} \Big|_{r=0} = 0 \quad \forall i \in [1, N] \quad (9)$$

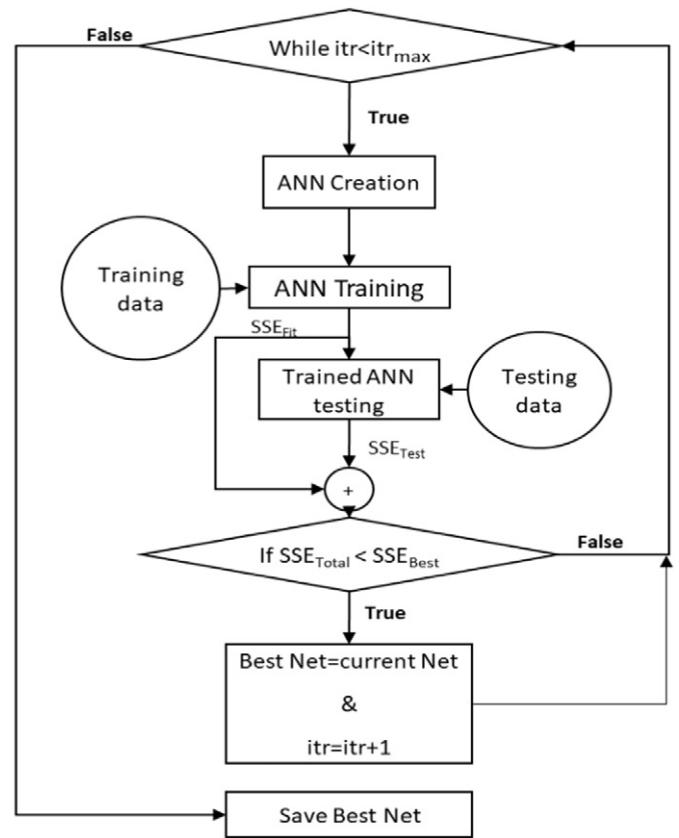


Fig. 2. ANN training data flow diagram.

$$q_i |_{r=R_p} = f(C_{1,2,...,N}) \quad (10)$$

Equation (9) is a result of symmetry at  $r = 0$  and equation (10) is based on the assumption that instantaneous equilibrium exists at the solid-liquid interface.  $f(C)$  therefore is given by the isotherm model used (either Equation (3) or (4) as appropriate). The initial conditions for equations (6) and (8) are:

$$q_i = 0 \quad \forall r \in [0, R_p] \& i \in [1, N] \quad (11)$$

$$C_i = C_{o,i} \quad \forall i \in [1, N] \quad (12)$$

HSDM was coded as a function which solves the partial differential equations, using the method of lines, for a given set of  $D_s$  values. MATLAB's built-in *ode15s* routine was used to integrate the differential equations. The function returned SSE between the model predicted percentage removal values and the experimentally obtained removals.

After running the simulations, the average solid loading at any time  $t$ ,  $q_t$ , is given by the material balance equation

$$\frac{m_A}{V_L} q_t = C_o - C_t \quad (13)$$

The percentage removal  $R$  was calculated as follows.

$$R = \frac{C_o - C_t}{C_o - C_e} \times 100 \quad (14)$$

At equilibrium, the solid loading,  $q_e$ , may be calculated from Equation (13), using the equilibrium isotherm model. It may be noted here that  $R$  is defined relative to the equilibrium limit  $C_e$  and not as an absolute percentage involving the ratio of  $C_t$  to  $C_o$ . This is more realistic and a practical index as  $C_t/C_o$  of zero is never achieved due to equilibrium limitations.

When the HSDM was used to estimate the parameters, viz.  $D_{s,i}$  ( $i = 1, 2, \dots, N$ ), the error criteria was based on the percentage removal of all the  $N$  components in the mixture at  $n_p$  data points as shown in Equation (15), which was minimized using a suitable

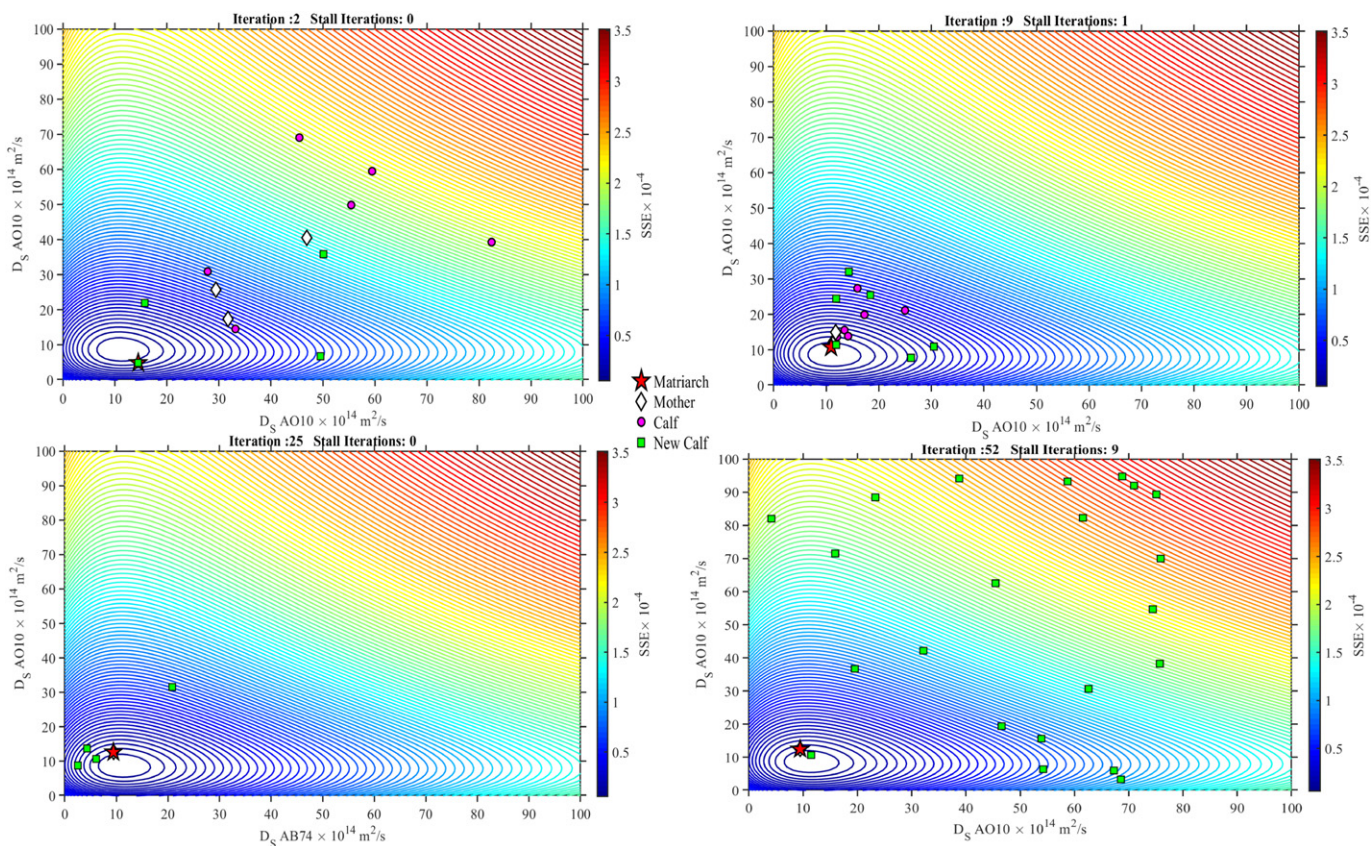


**Fig. 3.** A representative EHO illustration for a binary adsorption system. The elephants (search entities) traverse the domain ( $D_s$  parameter space) to reach the best watering hole (minimum SSE).

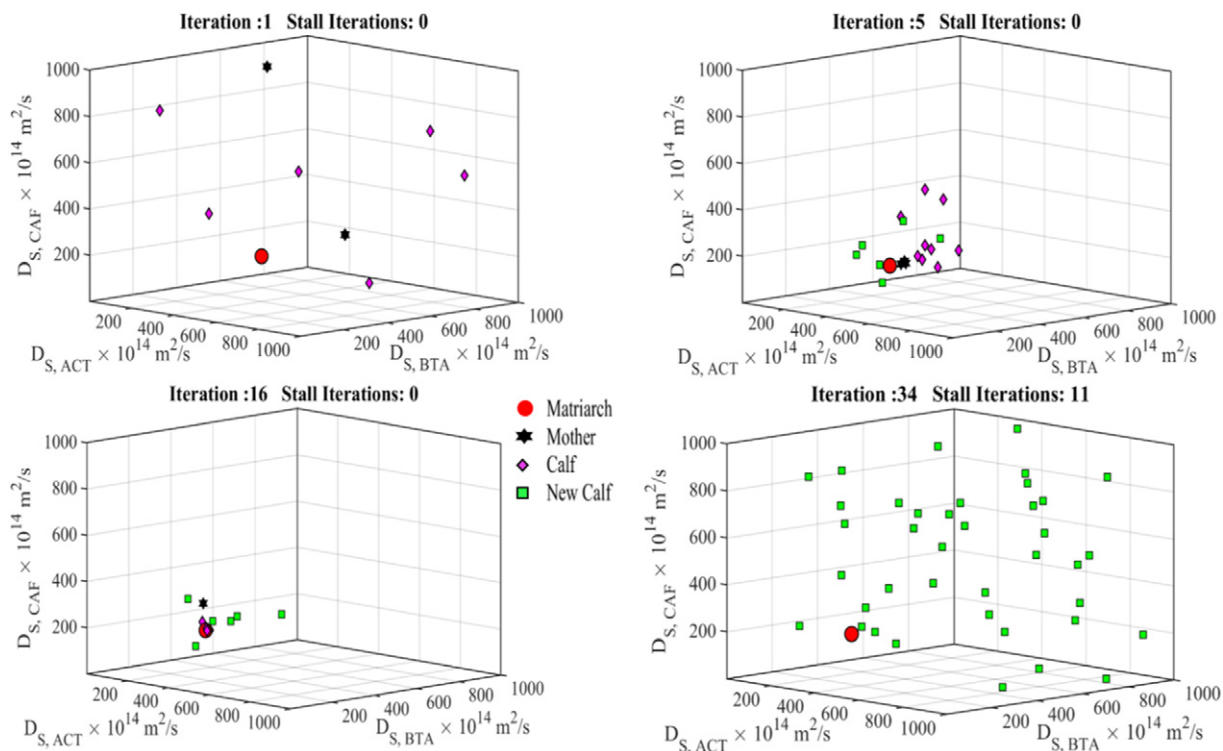


**Fig. 4.** A representative EHO illustration for a ternary adsorption system. The elephants (search entities) traverse the domain ( $D_s$  parameter space) to reach the best watering hole (minimum SSE).

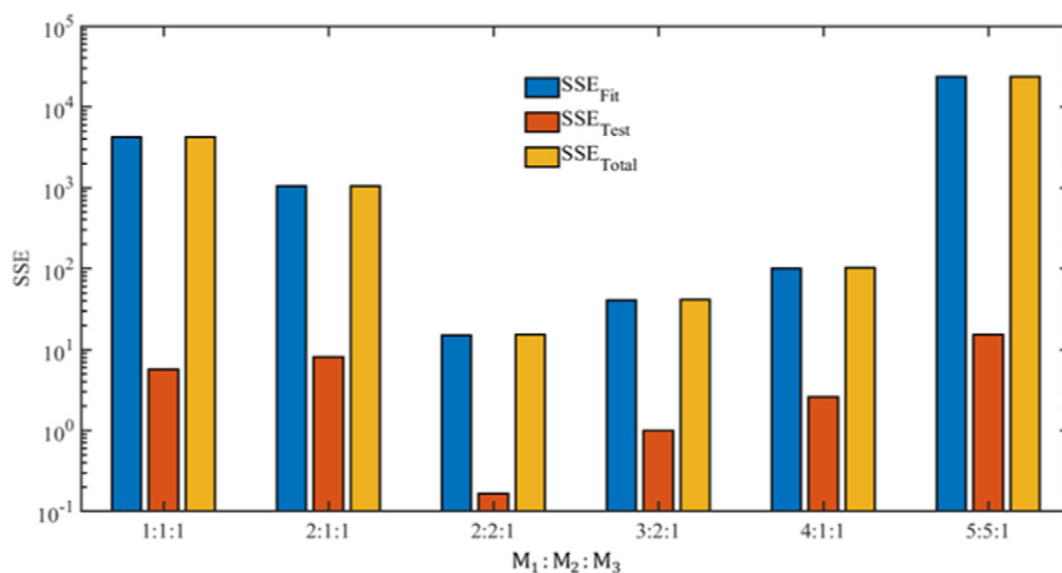


Fig. 5. Variation of SSE with neuron ratio in the hidden layers for the single component system. The number of neurons used were lowest multiples of 5.

optimization algorithm described in section 2.3.5 to obtain the best  $D_s$  vector.

$$SSE = \sum_{i=1}^N \sum_{j=1}^{n_D} (R_{i,Exp} - R_{i,Fit})^2 \quad (15)$$

### 2.3. Artificial neural network (ANN)

#### 2.3.1. ANN specifications

ANN was setup in MATLAB® 2019a. As it is proposed that ANN is to replace HSDM, it must replicate the HSDM simulations with fidelity. Therefore, a Fitnet, a type of feed forward neural network available in MATLAB for data regression, was chosen. The ANN used for current work consisted of 5 layers, viz. 1 input layer, 3 hidden layers and 1 output layer with different number of neurons in each of the hidden layers ( $M_i$ ) as shown below in Fig. 1. The transfer function of the output layer is linear (*purelin*) while those in the hidden layers are hyperbolic tangent sigmoid (*tansig*).

The training was done using MATLAB *train* function. This function divided training data in ratio of 90:5:5 for training, testing and validation respectively. Levenberg Marquart algorithm was implemented for training. The performance criterion was Sum of Square of Errors (SSE), defined according to Equation (15). A maximum epoch of 1000 training cycles was set. The data here corresponds to time vs R data at various conditions given in Table 2.

#### 2.3.2. Identifying the optimum number of neurons in each hidden layer

The number of neurons in each layer was fixed by identifying two parameters viz. i) ratio of number of neurons in each of the hidden layers i.e.  $M_1 : M_2 : \dots : M_i$  and ii) number of neurons in each hidden layer at the optimum neuron ratio in the hidden layers. To obtain the optimum number of neurons, the ANN was trained first with different ratios of neurons in the hidden layers. Once the optimum ratio with corresponding minimum SSE was identified, the ANN was then trained with varying total number of neurons in all the hidden layers until the lowest SSE was obtained.

#### 2.3.3. Training data generation

ANN is better at prediction and learning complex relationship patterns if a sizeable set of training data is made available at different conditions. Performing batch adsorption experiments at various combinations of conditions for training the ANN is unwieldy and practically difficult. Also, as the objective of the ANN is to replace HSDM simulations, the training data for ANN may be generated by running HSDM several times under different representative conditions of initial concentrations, pH, adsorbent dosage and time interval with realistic  $D_s$  parameters. By doing so, a large kinetic data set may be generated for training a system involving a known adsorbent and its identified isotherm for a given set of adsorptives under investigation. 100 datasets for each of the single, binary and ternary systems were simulated rigorously using HSDM as per conditions, given in Table 2. For each condition chosen, the plausible combination of  $D_s$  values, falling within the expected range of orders of magnitude, was input to the HSDM. The aqueous phase equilibrium concentration data ( $C_e$ ), input to the ANN, is also used for computing R (equation (14)).

#### 2.3.4. ANN training

In the current work, the ANN was trained with HSDM simulated data, which has negligible numerical noise and free from random errors usually associated with experimental data. Therefore, it was decided to additionally enhance the ANN's training with very limited actual experimental data. The procedure is as follows.

The ANN was first trained to minimize the SSE of ANN fit ( $SSE_{Fit}$ ) with HSDM simulated data. This ANN was additionally checked to see whether its predictions fitted well with one randomly chosen experimental kinetic run for each of the systems. In this run, surface diffusivities had already been estimated using HSDM and the same values were input to ANN. The error between the experimental data and the ANN prediction is used to find  $SSE_{Test}$ . The sum of  $SSE_{Fit}$  and  $SSE_{Test}$  viz.  $SSE_{Total}$  were then minimized. We term such an ANN as completely trained. To the best of our knowledge, this approach does not seem to have been implemented before for ANN studies involving adsorption. The algorithm implemented for training the ANN, is represented in Fig. 2. The ANN is initialized with random weights and biases when training iteration count (*itr*) is less than the maximum training iteration count (*itr<sub>max</sub>*) since the  $SSE_{Total}$  had changed. The  $SSE_{Total}$  is computed and compared with the best SSE ( $SSE_{Best}$ ) until the current iteration. If the current  $SSE_{Total}$  is less than the  $SSE_{Best}$  the *itr* is appended by 1 and the ANN is saved or else the ANN is reinitialized with random weights and process is repeated again until *itr* reaches *itr<sub>max</sub>*.

#### 2.3.5. Performance test of HSDM trained ANN with experimental data

The performance of ANN when dealing with experimental kinetics data gathered in-house and summarized in Table 2 was evaluated next. For the ternary system, performances of two different activated carbons (AC-II and MAC-II) were studied. The  $D_s$  values estimated from the completely trained ANN acting as surrogate to the rigorous HSDM were compared with those estimated using the actual HSDM itself. The same experimental data sets were used in both cases.

Elephant Herd Optimization (EHO) algorithm was implemented to obtain the vector of  $D_s$  parameters for each system. EHO [19] is a new initial guess free optimization algorithm developed in-house and is based on the behaviour of elephants. It utilizes the social hierarchy of elephants, where the Matriarch takes the herd to the best watering hole in her memory. The other mother elephants follow the matriarch. The calves of the herd follow their mother as shown in Figs. 3 and 4. The animated versions of the EHO searches for binary and ternary systems are provided as supplementary information in the form of mp4 file.

Supplementary video related to this article can be found at <https://doi.org/10.1016/j.molliq.2019.111888>

The search entities in EHO are the elephants and the watering hole corresponds to SSE in the current work. The size of watering hole is proportional to the inverse of SSE and its coordinates in the N-dimensional space represent the magnitudes of the vector of estimated parameters ( $D_s$ ). Stall iterations correspond to the number of successive iterations since the matriarch had found a better waterhole than the current global best water hole. Higher the stall iterations, greater is the number of new calves born and wider the search area of new calves (Figs. 3 and 4). Further details on the efficiency and accuracy of EHO are detailed in Gopinath and Aravamudan [19]. The required inputs to EHO are the number of search entities (mother elephants and calves) and limits of the search domain. The number of search elephants was 6 mother elephants and 5 calves per mother. The

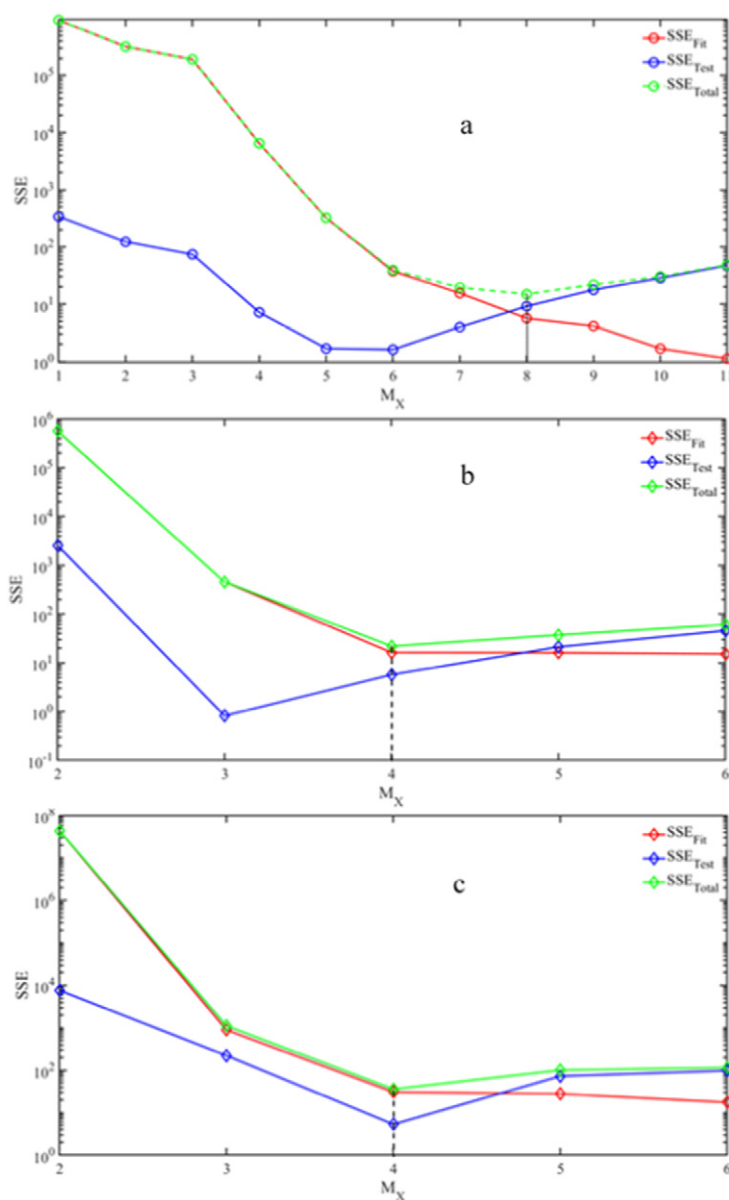


**Fig. 6.** ANN performance as a function of the integral multiplier  $M_x$  for a) single component b) binary component and c) ternary component system with optimum neuron ratio as given in Table 3.

search domain for  $D_s$  was set in the range from  $10^{-11}$  m<sup>2</sup>/s to  $10^{-15}$  m<sup>2</sup>/s based on values observed in literature [37].

### 3. Results and discussion

#### 3.1. Effect of ANN parameters

The isotherm parameters are provided as supplementary material in Tables S-1, S-2 & S-3. The optimum ratio of neurons in hidden layers ( $M_1 : M_2 : M_3$ ) was found iteratively.

The variation of SSE with the neurons ratio for a single component adsorption system is shown in Fig. 5.

The ratio 2:2:1 was observed to give the best  $SSE_{Total}$  for the single component system. The total number of neurons which gave the lowest  $SSE_{Total}$  for the identified optimum ratio, was found by trial and error. Even though  $SSE_{Test}$  was at least an order of magnitude lower than  $SSE_{Fit}$  for most cases (Fig. 5), it still exerted a sizeable influence on the parameter estimation using ANN as will be further discussed below. The variation of  $SSE_{Total}$ ,  $SSE_{Fit}$  and  $SSE_{Test}$  with the scaling factor  $M_x$  is given in Fig. 6.

The optimum  $M_x$  value is 8 for single component system. It may be observed that the  $SSE_{Fit}$  decreases monotonically with increasing number of neurons but  $SSE_{Test}$  passes

**Table 3**  
Number of neurons per hidden layer for different adsorption systems.

System	$M_1 : M_2 : M_3$	$M_x$	$SSE_{Fit}$	$SSE_{Test}$	$SSE_{Total}$	Total Training time (mins)
Single	2:2:1	8	5.67	9.17	14.84	12
Binary	4:3:2	4	5.73	16.27	22.00	28
Ternary	5:3:2	4	5.34	30.66	36.00	55

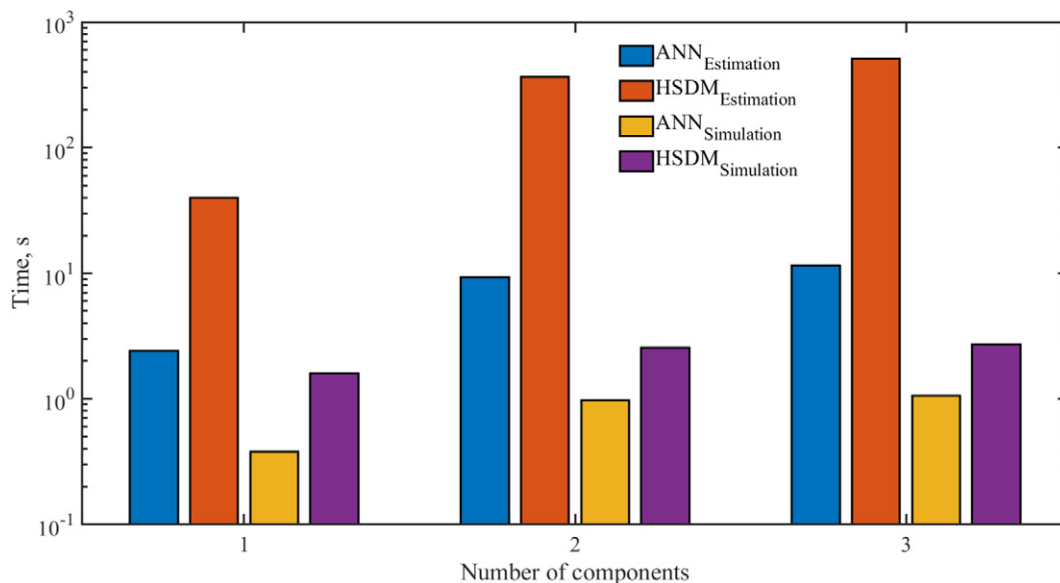


Fig. 7. Variation of average computational time for estimating parameters and for one simulation using ANN and HSDM for different adsorption systems.

through a distinct minimum with increasing number of neurons. This may be attributed to over-parametrization of ANN with increasing number of neurons which seems to retard the predictive capabilities of ANN. The number of neurons corresponding to minimum  $SSE_{Total}$  is used. At such conditions, it is remarkable to note that the  $SSE_{Test}$  which is based on just a single data set has an SSE that is comparable to  $SSE_{Fit}$  which was based on 100 data sets. If emphasis had been placed on only the lowest value of the  $SSE_{Fit}$  and an inordinately large number of neurons had been chosen, say 11, the computation effort would have increased.  $SSE_{Test}$  would suffer and the  $D_s$  parameters that were estimated by ANN would compare only poorly with those obtained from rigorous HSDM estimation. Three ANNs were trained successfully, for single, binary and ternary adsorption kinetics, using data simulated by solving HSDM for plausible  $D_s$  values for conditions specified in Table 2. The results are summarized in Table 3.

In addition to the neuron ratio and  $M_x$ , the  $SSE_{Total}$  and total ANN training time are also reported. The training time includes the time required for generating training data from HSDM simulations and for complete training of the ANNs developed for single, binary and ternary adsorption kinetics.

### 3.2. Computational efficiency of ANN

EHO was able to estimate the parameters rapidly with a smaller number of iterations and computational time. The computational times for execution for the rigorous HSDM and its ANN surrogate are compared in Fig. 7. The computational time required for estimating  $D_s$  values using the completely trained ANN surrogate is on average, 14 times lower per simulation and 16 times lower for overall estimation when compared to HSDM. Furthermore, it may be seen from Fig. 7, the time requirement for HSDM estimation increases almost exponentially with increasing number of components. This will considerably delay the parameter estimation by HSDM as the number of iterations required will be higher. The completely trained ANN simulation times are significantly lower even when the number of components increase. This may be attributed to the fact that ANN need not solve partial differential equations numerically as required in HSDM.

Also, once the system is trained, the network does not alter with every simulation and hence, the variation in simulation time is smaller when compared to HSDM. During parameter evaluations involving HSDM if  $D_s$  values used by the optimizer happen to be far from the actual  $D_s$  values, then the system may become stiff and integration would take a long time. Thus, the duration and variation in parameter estimation times for HSDM are high.

### 3.3. Accuracy of ANN predictions

It is not sufficient that the ANN surrogate is faster than the HSDM. It should enjoy comparable accuracy as well for it to have credible predictive and parameter estimation capabilities under different operating conditions. Plots of SSE obtained using HSDM and its completely trained ANN surrogate for the single component (Run 4 of Table 2), binary (Run 2 of Table 2) and ternary systems (Run 7 of Table 2) are shown in Fig. 8. It may be seen from Fig. 8, that ANN closely follows HSDM.

The parity plot between  $D_s$  values estimated using ANN and HSDM is shown in Fig. 9(a). The estimations made by ANN shows fidelity with HSDM estimations as evidenced from the parity plot. This suggests that the completely trained ANN

surrogate for HSDM is competent to estimate the parameters of the new experimental kinetics data sets at different operating conditions and the estimated  $D_s$  values are very close to those estimated by using HSDM, estimated parameters are given in Table S-4 of the supplementary material. It is emphasized that the ANN had not been trained *a priori* with these new experimental data sets. We also decided to check what would have happened if ANN was not completely trained i.e. was not tested with experimental data (section 2.3.4). The  $D_s$  values from incompletely trained ANN were significantly different from the values estimated from HSDM as shown in Fig. 9(b).

### 3.4. Performance of ANN at untrained process conditions

The completely trained ANN, trained for conditions given in Table 2, was used to estimate parameters for a completely new run. The conditions for this run (single component system at 35 °C, pH 6,  $m_A/V_L$  of 1.2 g/L and  $C_o$  of 200 mg/L) was within the bounds of process conditions detailed in Table 2. ANN was not trained using any of these conditions. The fit predicted by the ANN surrogate to the experimental kinetic data is given in Fig. 10. ANN was able to fit reasonably well with the experimental data. Moreover, the  $D_s$  values estimated using ANN was similar to the  $D_s$  estimated using HSDM. This indicates that ANN surrogate, once completely trained, is reliable to predict adsorber performance at intermediate conditions where experimental data are not available. This may translate into reliable process optimization, removing the necessity of time consuming and expensive additional experimentation thereby entailing considerable saving of resources.

ANN, acting as a surrogate to the HSDM, could capture the kinetics with its estimated diffusivity parameters. The objective of tuning the ANN was to identify the best combination which can not only fit the training data but also the testing data. Each neuron consists of a transfer function which transforms the input signal to an output signal. Hidden layers consist of collection of neurons in each layer, which resolve the input signal to identify more complex features of the input data. In the current work, the hidden layer identifies the features in data due to pH, T,  $C_o$ , dosage,  $C_e$ ,  $D_s$  and time. Due to multiple hidden layers the features exhibited by these parameters on the percentage removal of adsorptive is captured more accurately. This feature of ANN enables it to give due importance to each and every input variable and effect of all the parameters could be observed.

### 3.5. Comparison OF PFO, PSO, HSDM and ANN

For comparison with HSDM, the pseudo first and second order models were fit to the percentage removals as a function of time. The test conditions are given in Table 4.

The fits are shown in Fig. 11. The equilibrium value  $C_e$  required for computing percentage removal (equation (14)) is obtained from the material balance relation (equation (13)). In case of PSO and PFO (equations (1) and (2))  $q_e$  values were estimated by fitting the PFO and PSO models to the experimental C versus t data. The model parameters estimated are the kinetic constants  $k_1$  or  $k_2$  and  $q_e$  values. In the case of HSDM and ANN,  $C_e$



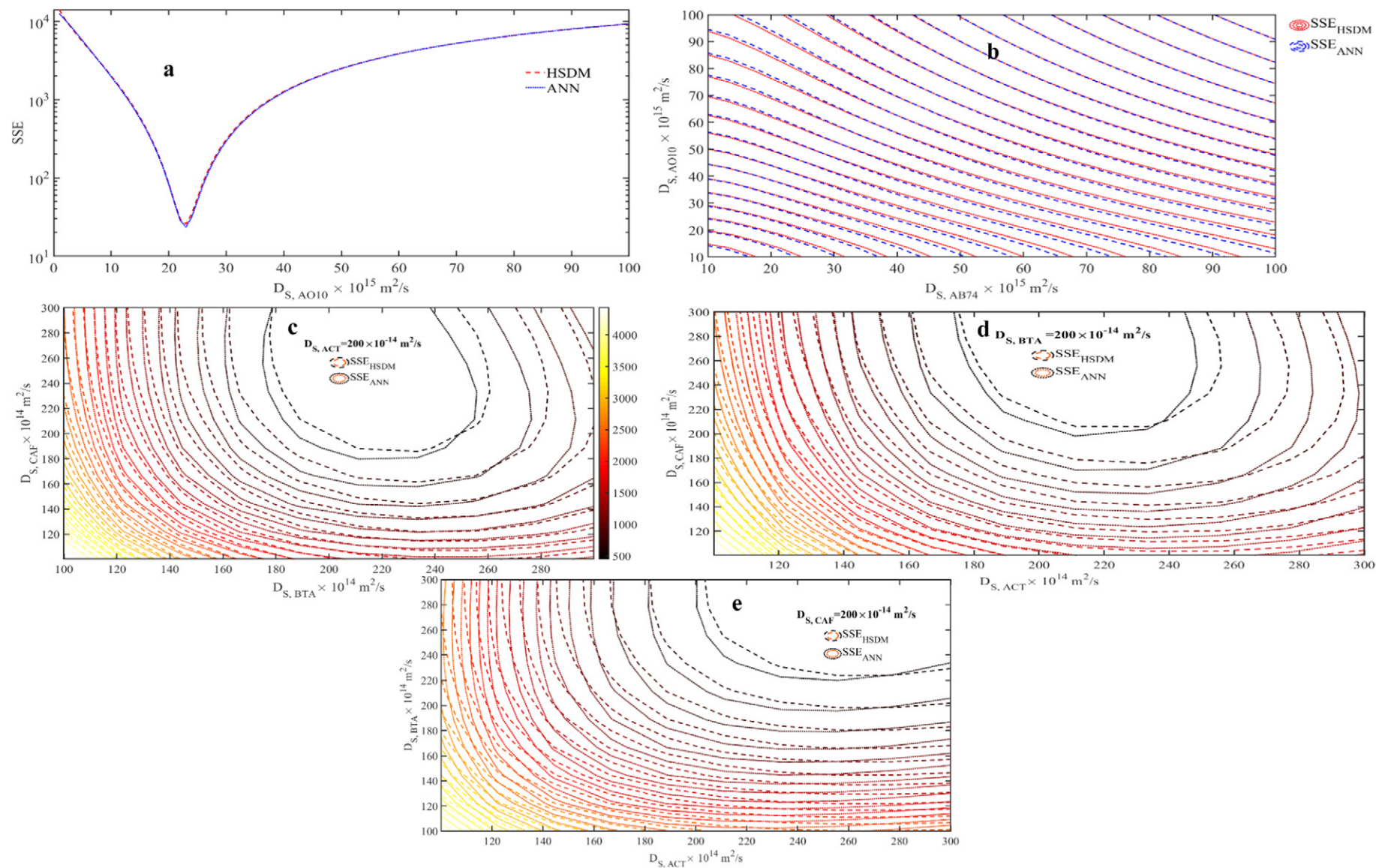


Fig. 8.  $D_s$  vs SSE obtained by ANN and HSDM for a) Single component System b) binary and c-e) ternary system.

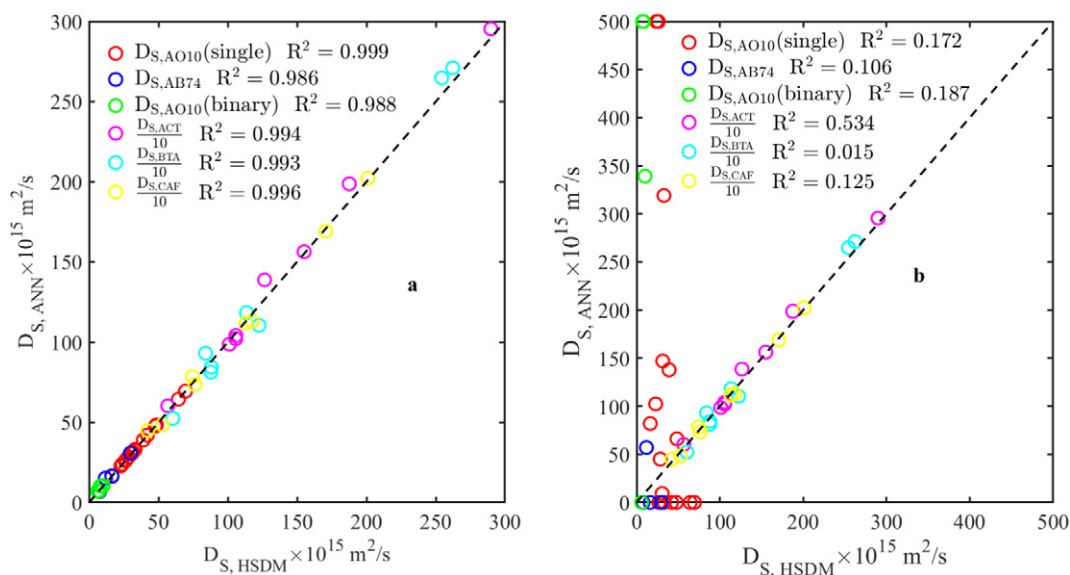


Fig. 9. Comparison of ANN estimated  $D_s$  values and HSDM Estimated  $D_s$  values using ANNs trained a) with testing and b) without testing using an experimental dataset.

values were computed by solving equation (13) using the isotherm relation between  $q_e$  and  $C_e$ . The parameters estimated by different models are summarized in Table 5.

It may be seen that HSDM and its ANN surrogate capture the percentage removal trends accurately, reaffirming that the completely trained ANN captures the HSDM accurately. These two approaches are based on actual equilibrium data which were represented with appropriate isotherm fits (equations (3) & (4)). However, PFO and PSO only estimated the equilibrium loadings ( $q_e$ ) values directly from the kinetics data and these are quite different from actual equilibrium values (Table 5). Interesting trend is visible from the Fig. 11. The pseudo-order models, especially the PSO tends closer to the HSDM predictions under conditions where the adsorption kinetics was rapid. This may be observed at initial times for all systems. For AB74 in the binary system, and for BTA and CAF for the ternary systems, where the kinetics are relatively faster than the other components, the corresponding PSO predictions are closer to the HSDM fits. It may be inferred that the estimation of  $q_e$  by the PSO is relatively more accurate when the kinetics are fast thereby enabling the concentration data at later times to be closer to actual equilibrium. During initial times, the internal diffusion effect is not yet manifest and only external transport limitations come into play. However, the applicability of PFO and PSO may not be generalized at all times and to all

species. These indicate that internal diffusion may act as a key mechanism in adsorption kinetics which should not be overlooked when multicomponent mixtures involving different types of species are analysed.

### 3.6. Mechanisms associated with adsorption kinetics

#### 3.6.1. A. single component adsorption

Guo and Wang [36] applied the Langmuir adsorption kinetics rate expression and deduced conditions for applicability of the PFO and PSO models. PFO model was applicable at initial times, negligible active sites occupation on the adsorbent and high feed concentration  $C_0$  in the fluid phase. Under these conditions, they showed that the PSO transformed into the PFO model. PSO model was shown to be applicable at final stages of adsorption, low feed concentration and nearly complete active sites occupation. They concluded that when only few active sites are present, transport factors rather than kinetic ones dominate the adsorption process. The mechanistic discussion on the transport within the adsorbent is given below.

Dimensionless concentration profiles (Figs. 12a and 13a) and fluxes of adsorbates (Figs. 12b and 13b) are given for single component system for runs 12 and 4 (Table 2). These are influenced by the equilibrium loading at the interface and the surface diffusivity.

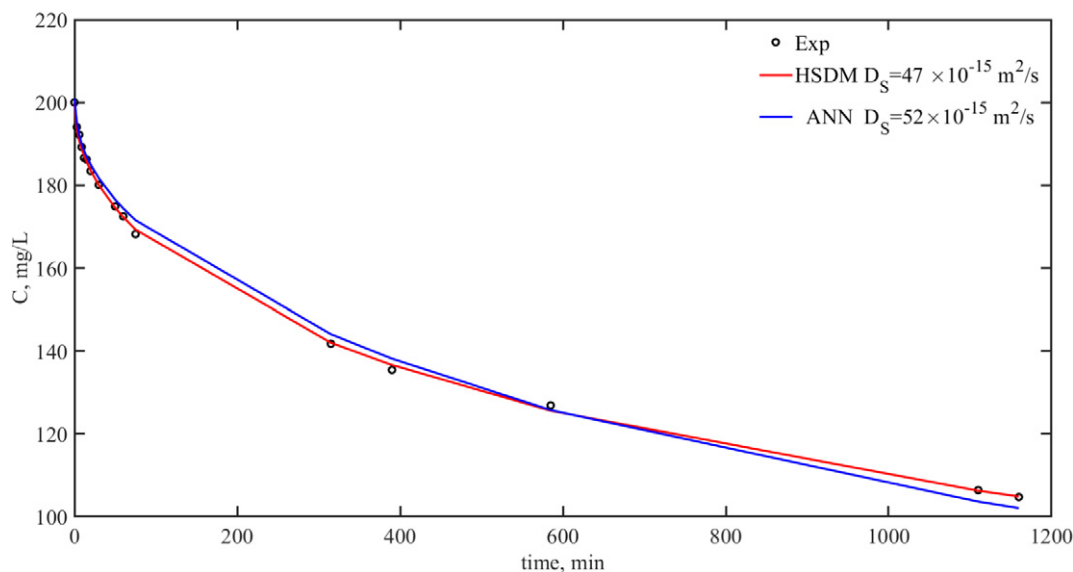


Fig. 10. ANN Fit with single component experimental data at untrained process conditions i.e.  $35^\circ\text{C}$ , pH 6,  $\frac{m_A}{V_L}$  of 1.2 g/L and  $C_0$  of 200 mg/L.

**Table 4**  
Conditions of comparison of PFO, PSO, HSDM and ANN.

System	Carbon	T, °C	pH	$\frac{m_A}{V_L}$ , g/L
Single	AC	25	4	1.6
Binary	AC	35	4	1.6
Ternary	MAC	44	3	2

Adsorbate fluxes (Figs. 12b and 13b) near the surface tend to be higher as the interfacial loading is the highest (concentration effect). The adsorbate concentrations (Figs. 12a and 13a) decline rapidly from the interface and hence the flux increases (concentration gradient effect). The loci of radial distances inside the adsorbent where the fluxes are maximum are shown in the figures.

As the radial distance inside the solid interface increases, adsorbate concentration values become smaller and they decrease more gradually. These contribute to a distinct decrease in the concentration gradients. Hence, the flux declines after passing through a maximum. Further, if the diffusivity of the adsorbate is high, it penetrates faster causing the adsorbate profiles to broaden thereby reducing the fluxes (solute diffusion effect). With increasing time, the liquid concentration decreases at the interface and so does the equilibrium adsorbent loading. Hence the fluxes also decline with time.

Temperature increases the surface diffusivity in run 12 by around 30% when compared to run 4 (Table S-3). Hence there is more penetration of the adsorbate in run 12 than in run 4 (Figs. 12(a) and 13(a)). However, this increase in diffusivity is not high enough for the profile to spread considerably into the adsorbent in run 12. Additionally, there is a higher equilibrium loading of the dye at the interface in this run and these contribute to higher fluxes than run 4.

3.6.2. B. binary adsorption

PFO and PSO models are applicable for systems which do not exhibit competitive adsorption. Hong et al. [52] have stated that it is doubtful whether the pseudo kinetic models that have been proposed for single component adsorption may also be extended to competitive multicomponent adsorption kinetics. Applying PFO and PSO to multicomponent systems may not provide

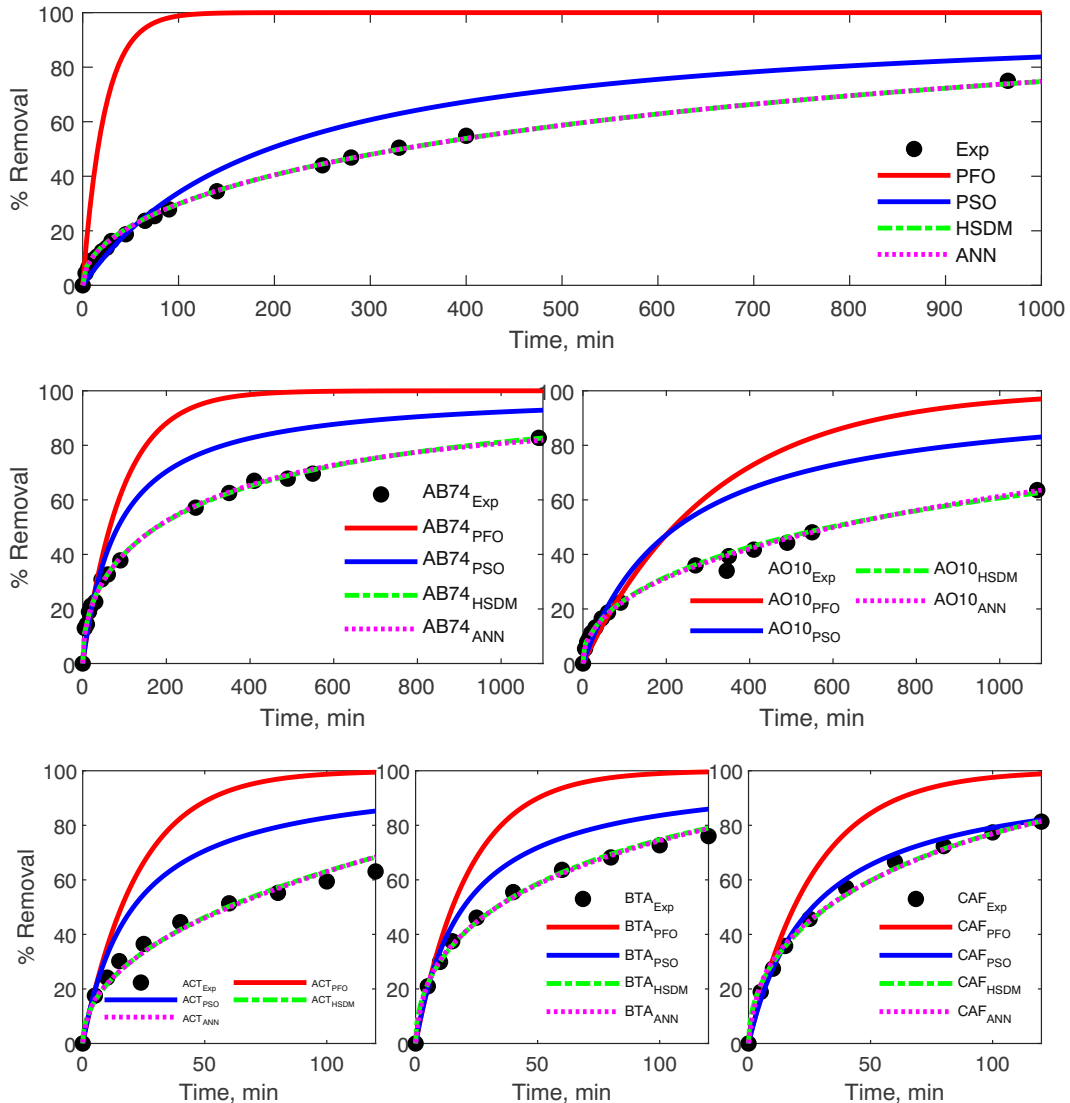


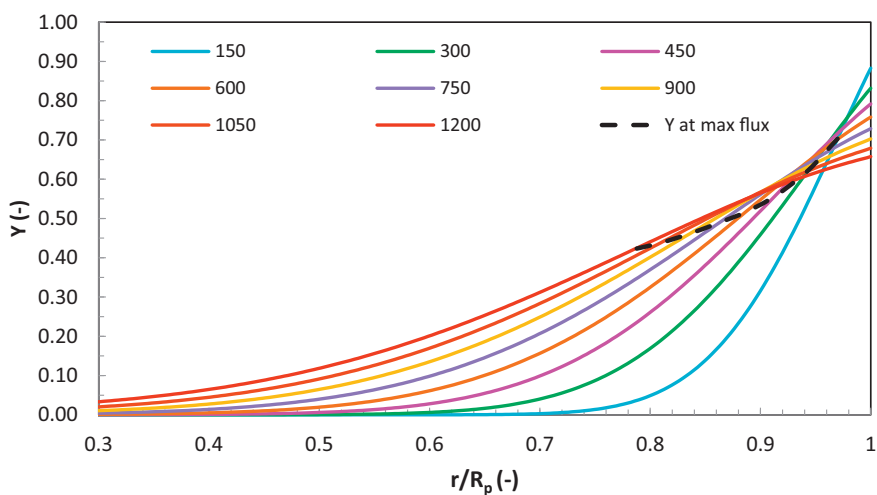
**Fig. 11.** Removal vs Time fits for PSO, PFO, HSDM and ANN for various systems given in Table 4.

**Table 5**  
Estimated parameters of different kinetic models for runs given in Table 4.

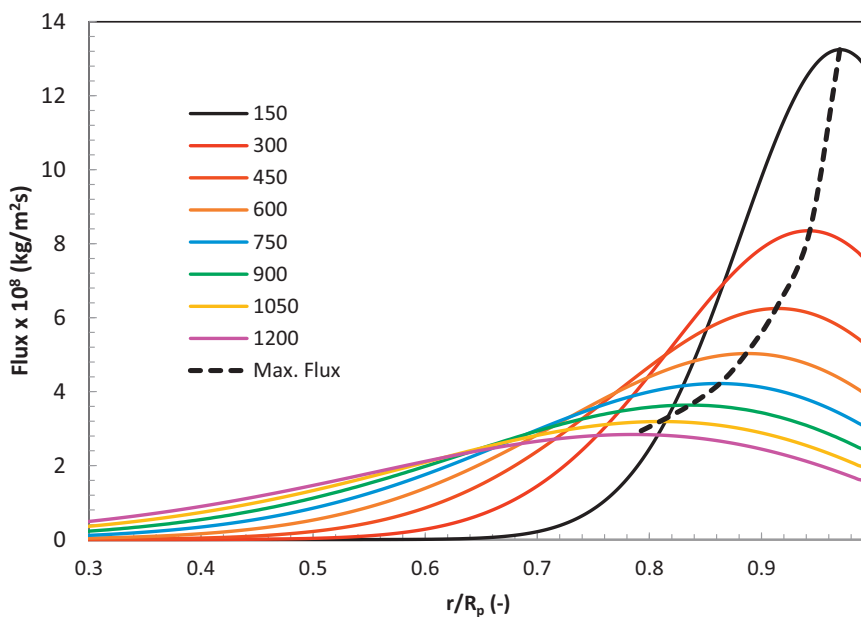
System	PFO		PSO		HSDM	ANN	$q_e$ Isotherm, mg/g
	$k_1 \times 10^4$ 1/min	$q_e$ mg/g	$k_2 \times 10^4$ g/mg-min	$q_e$ mg/g	$D_s \times 10^{15}$ m <sup>2</sup> /s	$D_s \times 10^{15}$ m <sup>2</sup> /s	
Single	44.11	45.02	0.97	53.00	2.28	2.28	61.16
Binary	106.44	20.59	4.99	23.77	1.64	1.98	28.78
	31.94	19.06	2.06	21.65	0.79	0.83	30.19
Ternary	379.67	33.32	14.67	32.808	198.60	187.58	46.33
	422.23	38.85	12.53	40.679	270.75	262.25	47.38
	306.07	49.78	8.00	47.481	169.33	170.74	48.91

accurate estimates of equilibrium adsorbent loading for all the components in the mixture and the kinetic constants would be implicit in the competitive effects. Rather, it is better to use the multicomponent isotherm to estimate the adsorbent equilibrium loading at the interface and use the mechanistic multi-component HSDM.

Dimensionless concentration profiles and fluxes of adsorbates are given in Figs. 14–15 corresponding to runs 1 and 4 (binary system, Table 2). Here, competition sets in between solutes vying for available active sites and a consequent noticeable decline in fluxes and penetration may be observed, when compared to the single component system. In run 1, acid blue has both faster kinetics and interfacial loading due to more favourable

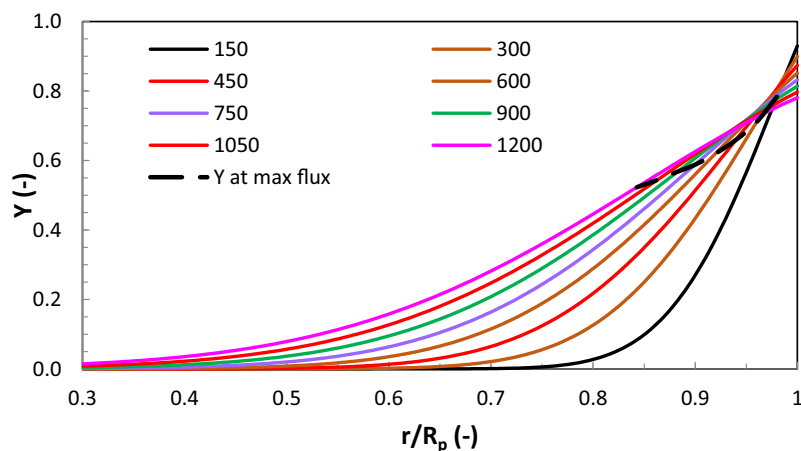


(a)

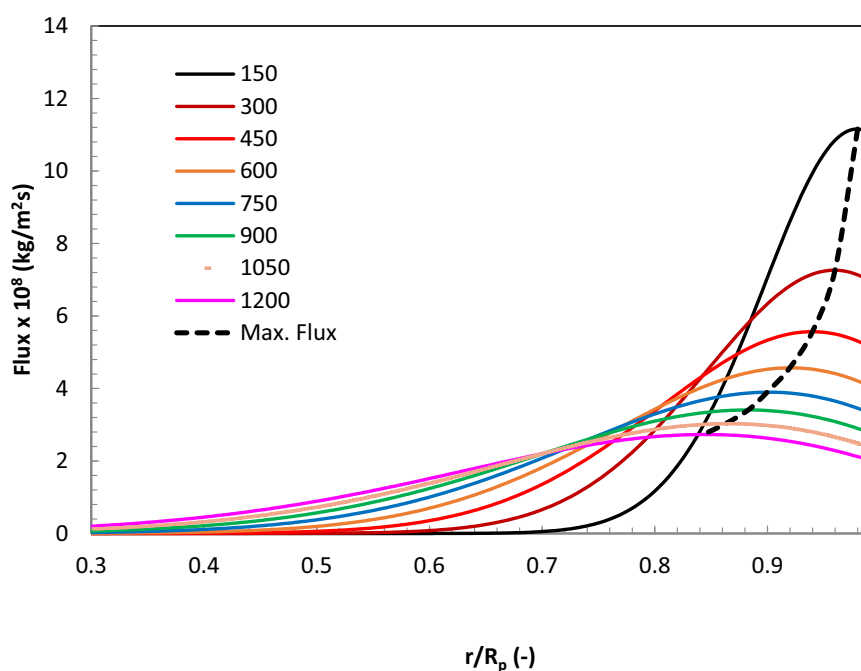


(b)

**Fig. 12.** (a) Dimensionless adsorbate concentration profiles (b) Flux profiles at different times (in minutes) corresponding to acid orange dye,  $C_0 = 100$  mg/L,  $m_A/V_L = 1.6$  g/L, pH = 4,  $T = 45$  °C,  $D_s = 28.5 \times 10^{-15}$  m<sup>2</sup>/s.



(a)



(b)

**Fig. 13.** (a) Dimensionless adsorbate concentration profiles (b) Flux profiles at different times (in minutes) corresponding to acid orange dye,  $C_0 = 100$  mg/L,  $m_A/V_L = 1.6$  g/L, pH = 4, T = 25 °C,  $D_s = 22.8 \times 10^{-15}$  m<sup>2</sup>/s.

isotherm than acid orange. As the diffusion coefficient for acid blue is nearly twice that of acid orange (Table S-4) there is considerable penetration of acid blue (Fig. 14(a)) when compared to acid orange (Fig. 14(b)). This however causes considerable spreading of the concentration profiles for acid blue when compared to acid orange, as shown in these figures. Hence, the fluxes are lower for acid blue (Fig. 14(c)) relative to acid orange (Fig. 14(d)).

In run 4, the penetration of acid blue (Fig. 15(a)) into the adsorbent is greater, but at the cost of reduced fluxes (Fig. 15(c)) when compared to the penetrations (Fig. 15(b)) and fluxes of acid orange (Fig. 15(d)). The diffusivity of acid blue dye is almost thrice as that of acid orange dye (Table S-4 binary system) and has higher surface loading as well. As the solute diffuses faster within the adsorbent, its peak adsorbate flux value will be found deeper within the adsorbent and the flux profile will be broader as well.

#### 4. Conclusions

HSDM trained ANN was successfully able to capture the kinetics of single, binary and ternary batch adsorption systems. HSDM based

ANN estimated HSDM parameters accurately and precisely with 14 times lesser computational time on average. The ANN was also able to simulate the kinetics, given the  $D_s$  parameters, with 99% similarity with HSDM simulations. Training data corresponding to only 100 simulations of HSDM augmented with just one experimental kinetic data set were sufficient enough to train the ANN of presented accuracy.

It was observed that even when the fits to experimental data are good, PFO and PSO are not able to capture the kinetics of the system accurately. Based on fits of PFO and PSO the time required for a particular percentage removal is significantly different from what is experimentally observed. PFO and PSO predicts the  $q_e$  values inaccurately for data which are far away from the equilibrium. Internal diffusion is a key mechanism in adsorption kinetics which should not be overlooked.

ANN trained by HSDM would be able to capture the effects of alteration in diffusional mass transfer in an adsorbent which would be

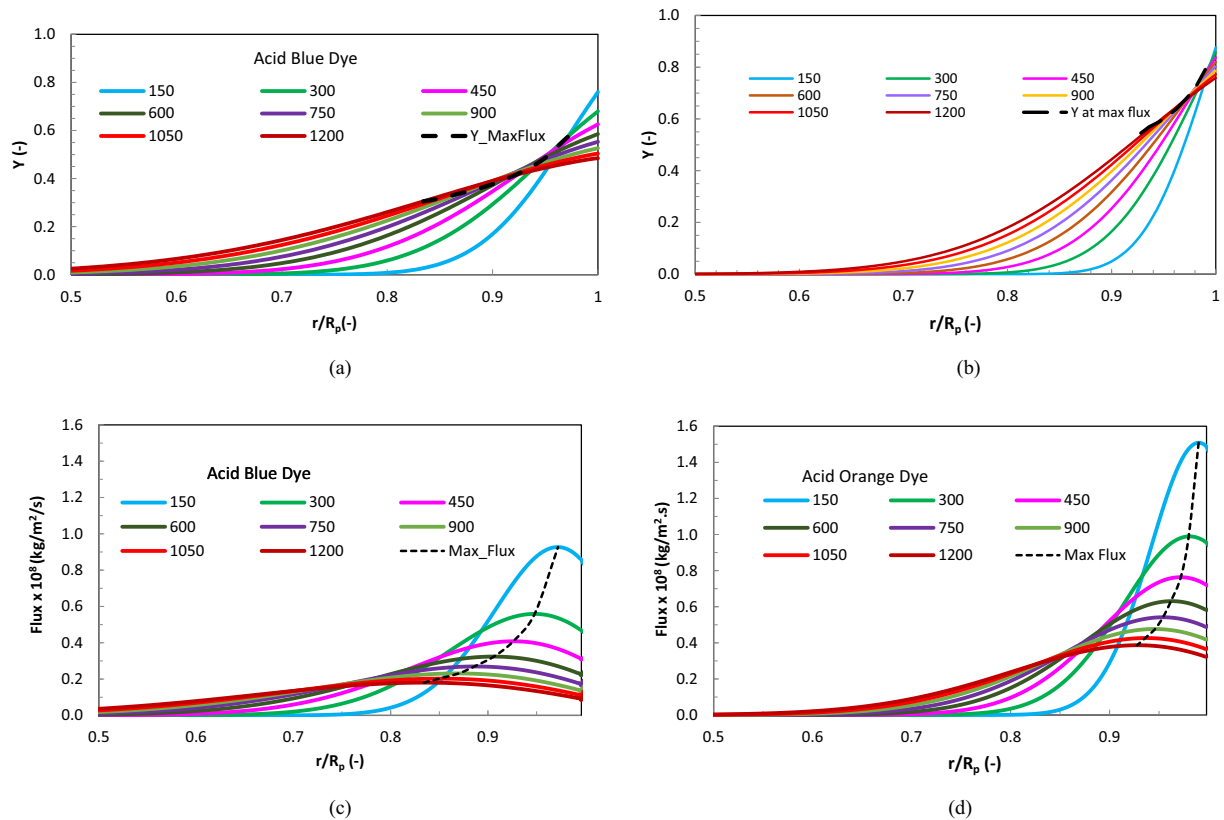


**Fig. 14.** Dimensionless adsorbate concentration profiles for (a) acid blue (b) acid orange and flux profiles for (c) acid blue and (d) acid orange at different times (in minutes) corresponding to  $C_{0,AB} = 50$  mg/L,  $C_{0,AO} = 50$  mg/L,  $m_A/V_L = 1.6$  g/L,  $pH = 4$ ,  $T = 35$  °C,  $D_s, AB = 16.5 \times 10^{-15}$  m<sup>2</sup>/s,  $D_s,AO = 8.1 \times 10^{-15}$  m<sup>2</sup>/s.

missed by ANNs trained with PFOM or PSOM. Therefore, the ANN trained by HSDM will give a more fundamental understanding of the kinetics. ANN would not be devoid of any physical meaning as it would be relating the process parameters with transport parameters as well. The author strongly recommends using HSDM or similar more rigorous diffusion-based models for capturing the adsorption kinetics and training of the any ANN surrogates.

More input parameters like point of zero charge, pH and different carbons may be used to extend the range of applicability of ANN. Owing to the significantly lower computational time in estimating parameters, HSDM based ANN may be deployed in continuous column kinetic analysis in a rigorous manner. In continuous columns the variation in process variables occur as a functions of column height, adsorbent radius and time. Solving the HSDM repeatedly would be computationally challenging.

The completely trained ANN is able to capture the effect of process parameters accurately. Hence, it may be deployed in industries that typically handle fluctuating inlet compositions and operating conditions, for the optimum operation of adsorption-based systems.

### Acknowledgements

This work was carried out as regular academic research and no external funding agencies were involved.

### Notations

AB	Acid Blue. —
AO	Acid Orange. —
$b_i$	Bias of $i$ th hidden layer. —

$C_0$	Initial solute concentration in liquid. $\frac{mg}{L}$
$C$	solute concentration in liquid. $\frac{mg}{L}$
$C_e$	Equilibrium solute concentration in liquid. $\frac{mg}{L}$
$D_s$	Surface diffusion coefficient. $\frac{m^2}{s}$
$Q_m$	Extended sips isotherm parameter. $\frac{mg}{g}$
$q$	Solid loading. $\frac{mg}{g}$
$q$	Average solid loading. $\frac{mg}{g}$
$q_e$	Equilibrium solid loading. $\frac{mg}{g}$
$q_{Exp}$	Experimentally obtained solid loading. $\frac{mg}{g}$
$q_{Fit}$	Model predicted solid loading. $\frac{mg}{g}$
$n_f$	Freundlich isotherm parameter. —
$k_s$	Extended sips isotherm parameter. $(\frac{L}{mg})^{\frac{1}{n_s}}$
$n_s$	Extended sips isotherm parameter. —
$M_i$	Number of neurons in $i$ th hidden layer. —
$M_X$	Least number of neurons in any hidden layer. —
$m_A$	Mass of adsorbent. g
$N$	Number of components. —
$n_i^j$	$j^{th}$ Neuron in $i^{th}$ hidden layer. —
$V_L$	Volume of liquid. L
$R$	% Removal. —
$R_p$	Particle radius. m
$r$	Radial vector. m
$T$	Temperature. °C
$t$	Time. s
$k_1$	PFO rate constant. $\frac{1}{s}$
$k_2$	PSO rate constant. $\frac{g}{mg \cdot s}$
$k_f$	Freundlich isotherm parameter. $(\frac{L}{mg})^{\frac{1}{n_f}}$

### Appendix A. Supplementary data

Supplementary data to this article can be found online at <https://doi.org/10.1016/j.molliq.2019.111888>.

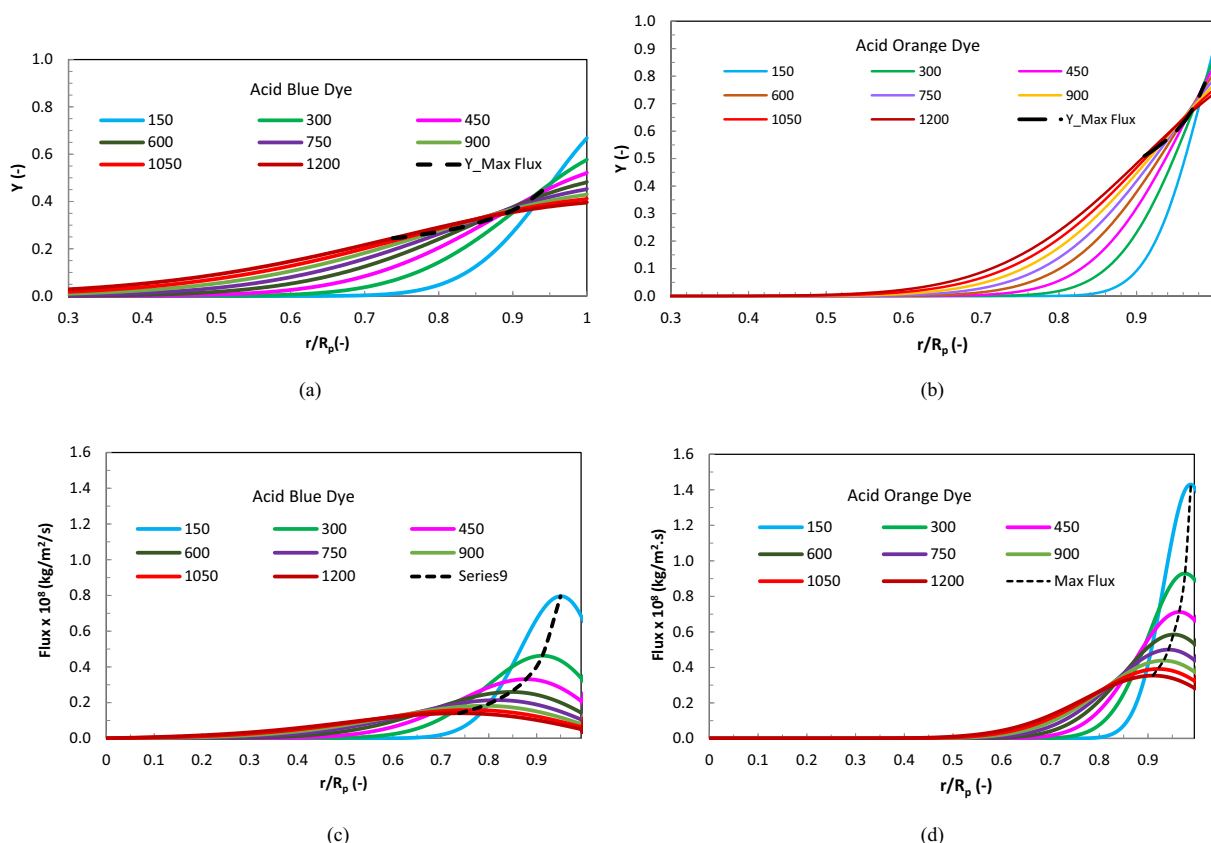


**Fig. 15.** Dimensionless adsorbate concentration profiles for (a) acid blue (b) acid orange and flux profiles for (c) acid blue and (d) acid orange at different times (in minutes) corresponding to  $C_{o,AB} = 50$  mg/L,  $C_{o,AO} = 50$  mg/L,  $m_A/V_L = 1.6$  g/L,  $pH = 8$ ,  $T = 35$  °C,  $D_{s,AB} = 29.7 \times 10^{-15}$  m<sup>2</sup>/s,  $D_{s,AO} = 10.2 \times 10^{-15}$  m<sup>2</sup>/s.

## References

- W. Li, B. Mu, Y. Yang, Feasibility of industrial-scale treatment of dye wastewater via bio-adsorption technology, *Bioresour. Technol.* 277 (2019) 157–170, <https://doi.org/10.1016/j.biortech.2019.01.002>.
- K. Sharma, R.K. Vyas, K. Singh, A.K. Dalai, Degradation of a synthetic binary dye mixture using reactive adsorption: experimental and modeling studies, *J. Environ. Chem. Eng.* 6 (2018) 5732–5743, <https://doi.org/10.1016/j.jece.2018.08.069>.
- D. Ceconet, D. Molognoni, A. Callegari, A.G. Capodaglio, Biological combination processes for efficient removal of pharmaceutically active compounds from wastewater: a review and future perspectives, *J. Environ. Chem. Eng.* 5 (2017) 3590–3603, <https://doi.org/10.1016/j.jece.2017.07.020>.
- R. Rostamian, H. Behnejad, A comprehensive adsorption study and modeling of antibiotics as a pharmaceutical waste by graphene oxide nanosheets, *Ecotoxicol. Environ. Saf.* 147 (2018) 117–123, <https://doi.org/10.1016/j.ecoenv.2017.08.019>.
- S. Sarkar, C. Bhattacharjee, Studies on adsorption, reaction mechanisms and kinetics for photocatalytic degradation of CHD, a pharmaceutical waste, *Ecotoxicol. Environ. Saf.* 121 (2015) 154–163, <https://doi.org/10.1016/j.ecoenv.2015.04.036>.
- C.-W. Cho, Y. Zhao, Y.-S. Yun, QSAR modelling for predicting adsorption of neutral, cationic, and anionic pharmaceuticals and other neutral compounds to microalgae *Chlorella vulgaris* in aquatic environment, *Water Res.* 151 (2019) 288–295, <https://doi.org/10.1016/j.watres.2018.12.033>.
- X.X. Liang, A.M. Omer, Z. Hu, Y. Wang, D. Yu, X. Ouyang, Efficient adsorption of diclofenac sodium from aqueous solutions using magnetic amine-functionalized chitosan, *Chemosphere* 217 (2019) 270–278, <https://doi.org/10.1016/j.chemosphere.2018.11.023>.
- A. Muthukumar, K. Aravamudan, Combined Homogeneous Surface Diffusion Model – design of experiments approach to optimize dye adsorption considering both equilibrium and kinetic aspects, *J. Environ. Manag.* 204 (2017) 424–435, <https://doi.org/10.1016/j.jenvman.2017.09.010>.
- A. Molla, Y. Li, B. Mandal, S.G. Kang, S.H. Hur, J.S. Chung, Selective adsorption of organic dyes on graphene oxide: theoretical and experimental analysis, *Appl. Surf. Sci.* 464 (2019) 170–177, <https://doi.org/10.1016/j.apsusc.2018.09.056>.
- Y. Gao, S.-Q. Deng, X. Jin, S.-L. Cai, S.-R. Zheng, W.-G. Zhang, The construction of amorphous metal-organic cage-based solid for rapid dye adsorption and time-dependent dye separation from water, *Chem. Eng. J.* 357 (2019) 129–139, <https://doi.org/10.1016/j.cej.2018.09.124>.
- S. Karmakar, D. Roy, C. Janiak, S. De, Insights into multi-component adsorption of reactive dyes on MIL-101-Cr metal organic framework: experimental and modeling approach, *Separ. Purif. Technol.* 215 (2019) 259–275, <https://doi.org/10.1016/j.seppur.2019.01.013>.
- S. Höhn, S. Virtanen, A.R. Boccacini, Protein adsorption on magnesium and its alloys: a review, *Appl. Surf. Sci.* 464 (2019) 212–219, <https://doi.org/10.1016/j.apsusc.2018.08.173>.
- A. Dąbrowski, Adsorption – from theory to practice, *Adv. Colloid Interface Sci.* (2001) [https://doi.org/10.1016/S0001-8686\(00\)00082-8](https://doi.org/10.1016/S0001-8686(00)00082-8).
- T. Esparza-Isunza, F. López-Isunza, Modeling Fixed-Bed Multicomponent Adsorption as a Step to Achieve Ultra-low Sulfur Diesel, Elsevier, 2015 <https://doi.org/10.1016/B978-0-444-63578-5.50110-9>.
- B.N. Bhadra, A. Vinu, C. Serre, S.H. Jhung, MOF-derived carbonaceous materials enriched with nitrogen: preparation and applications in adsorption and catalysis, *Mater. Today* (2018) <https://doi.org/10.1016/j.mattod.2018.10.016>.
- A.S. Alsaman, A.A. Askalany, K. Harby, M.S. Ahmed, A state of the art of hybrid adsorption desalination-cooling systems, *Renew. Sustain. Energy Rev.* 58 (2016) 692–703, <https://doi.org/10.1016/j.rser.2015.12.266>.
- F.H. Schünemann, M.E. Galárraga-Vinueza, R. Magini, M. Fredel, F. Silva, J.C.M. Souza, Y. Zhang, B. Henriques, Zirconia surface modifications for implant dentistry, *Mater. Sci. Eng. C* (2019) <https://doi.org/10.1016/j.msec.2019.01.062>.
- M. Talha, Y. Ma, P. Kumar, Y. Lin, A. Singh, Role of protein adsorption in the bio corrosion of metallic implants – a review, *Colloids Surfaces B Biointerfaces* 176 (2019) 494–506, <https://doi.org/10.1016/j.colsurfb.2019.01.038>.
- A. Gopinath, K. Aravamudan, A novel, initial guess free optimization algorithm for estimating parameters of batch kinetics model used to simulate adsorption of pollutant molecules in aqueous streams, *J. Mol. Liq.* 275 (2019) 510–522, <https://doi.org/10.1016/j.molliq.2018.11.015>.
- K. Wu, Y. Li, T. Liu, Q. Huang, S. Yang, W. Wang, P. Jin, The simultaneous adsorption of nitrate and phosphate by an organic-modified aluminum-manganese bimetal oxide: adsorption properties and mechanisms, *Appl. Surf. Sci.* 478 (2019) 539–551, <https://doi.org/10.1016/j.apsusc.2019.01.194>.
- A.M. Ghaedi, A. Vafaei, Applications of artificial neural networks for adsorption removal of dyes from aqueous solution: a review, *Adv. Colloid Interface Sci.* 245 (2017) 20–39, <https://doi.org/10.1016/j.cis.2017.04.015>.
- F. Ren, Z. Li, W.-Z. Tan, X.-H. Liu, Z.-F. Sun, P.-G. Ren, D.-X. Yan, Facile preparation of 3D regenerated cellulose/graphene oxide composite aerogel with high-efficiency adsorption towards methylene blue, *J. Colloid Interface Sci.* 532 (2018) 58–67, <https://doi.org/10.1016/j.jcis.2018.07.101>.

- [23] S. Qiao, X. Hu, Effect of pore size distribution shape on the prediction of binary adsorption equilibrium and kinetics of gases in activated carbon, *Separ. Purif. Technol.* 34 (2004) 177–189, [https://doi.org/10.1016/S1383-5866\(03\)00191-6](https://doi.org/10.1016/S1383-5866(03)00191-6).
- [24] S. Karimi, M. Tavakkoli Yaraki, R.R. Karri, A comprehensive review of the adsorption mechanisms and factors influencing the adsorption process from the perspective of bioethanol dehydration, *Renew. Sustain. Energy Rev.* 107 (2019) 535–553, <https://doi.org/10.1016/j.rser.2019.03.025>.
- [25] Y. Liu, W. Zhang, C. Zhao, H. Wang, J. Chen, L. Yang, J. Feng, W. Yan, Study on the synthesis of poly(pyrrole methane)s with the hydroxyl in different substituent position and their selective adsorption for Pb<sup>2+</sup>, *Chem. Eng. J.* 361 (2019) 528–537, <https://doi.org/10.1016/j.cej.2018.12.093>.
- [26] S. Chilukoti, T. Thangavel, Enhanced adsorption of Congo red on microwave synthesized layered Zn-Al double hydroxides and its adsorption behaviour using mixture of dyes from aqueous solution, *Inorg. Chem. Commun.* 100 (2019) 107–117, <https://doi.org/10.1016/j.inoche.2018.12.027>.
- [27] D. Jiang, M. Chen, H. Wang, G. Zeng, D. Huang, M. Cheng, Y. Liu, W. Xue, Z. Wang, The application of different typological and structural MOFs-based materials for the dyes adsorption, *Coord. Chem. Rev.* 380 (2019) 471–483, <https://doi.org/10.1016/j.ccr.2018.11.002>.
- [28] W. Gan, X. Shang, X.-H. Li, J. Zhang, X. Fu, Achieving high adsorption capacity and ultrafast removal of methylene blue and Pb<sup>2+</sup> by graphene-like TiO<sub>2</sub>@C, *Colloid. Surf. Physicochem. Eng. Asp.* 561 (2019) 218–225, <https://doi.org/10.1016/j.colsurfa.2018.10.079>.
- [29] S. Iftekhhar, D.L. Ramasamy, V. Srivastava, M.B. Asif, M. Sillanpää, Understanding the factors affecting the adsorption of Lanthanum using different adsorbents: a critical review, *Chemosphere* 204 (2018) 413–430, <https://doi.org/10.1016/j.chemosphere.2018.04.053>.
- [30] A. Syafuddin, S. Salmiati, J. Jonbi, M.A. Fulazzaky, Application of the kinetic and isotherm models for better understanding of the behaviors of silver nanoparticles adsorption onto different adsorbents, *J. Environ. Manag.* 218 (2018) 59–70, <https://doi.org/10.1016/j.jenvman.2018.03.066>.
- [31] A.A. Siyal, M.R. Shamsuddin, M.I. Khan, N.E. Rabat, M. Zulfqar, Z. Man, J. Siame, K.A. Azizli, A review on geopolymers as emerging materials for the adsorption of heavy metals and dyes, *J. Environ. Manag.* 224 (2018) 327–339, <https://doi.org/10.1016/j.jenvman.2018.07.046>.
- [32] A. Gupta, C. Balomajumder, Simultaneous adsorption of Cr(VI) and phenol onto tea waste biomass from binary mixture: multicomponent adsorption, thermodynamic and kinetic study, *J. Environ. Chem. Eng.* 3 (2015) 785–796, <https://doi.org/10.1016/j.jece.2015.03.003>.
- [33] A.M. Herrera-González, M. Caldera-Villalobos, A.-A. Peláez-Cid, Adsorption of textile dyes using an activated carbon and crosslinked polyvinyl phosphonic acid composite, *J. Environ. Manag.* 234 (2019) 237–244, <https://doi.org/10.1016/j.jenvman.2019.01.012>.
- [34] J.R. JJ, Simultaneous removal of binary dye from textile effluent using cobalt ferrite-alginate nanocomposite: performance and mechanism, *Microchem. J.* 145 (2019) 791–800, <https://doi.org/10.1016/j.microc.2018.11.047>.
- [35] W. Plazinski, W. Rudzinski, A. Plazinska, Theoretical models of sorption kinetics including a surface reaction mechanism: a review, *Adv. Colloid Interface Sci.* 152 (2009) 2–13, <https://doi.org/10.1016/j.cis.2009.07.009>.
- [36] X. Guo, J. Wang, A general kinetic model for adsorption: theoretical analysis and modeling, *J. Mol. Liq.* (2019) 111100, <https://doi.org/10.1016/j.molliq.2019.111100>.
- [37] E. Worch, *Adsorption Technology in Water Treatment: Fundamentals, Processes, and Modeling*, Walter de Gruyter, 2012 344, <https://doi.org/10.1515/9783110240238>.
- [38] M.G. Karlaftis, E.I. Vlahogianni, Statistical methods versus neural networks in transportation research: differences, similarities and some insights, *Transp. Res. C Emerg. Technol.* 19 (2011) 387–399, <https://doi.org/10.1016/j.trc.2010.10.004>.
- [39] S.S. Madan, K.L. Wasewar, S.L. Pandharipande, Modeling the adsorption of benzenoacetic acid on CaO<sub>2</sub> nanoparticles using artificial neural network, *Resource-Efficient Technologies 2* (2016) S53–S62, <https://doi.org/10.1016/j.reffit.2016.10.004>.
- [40] A.M. Ghaedi, S. Karamipour, A. Vafaei, M.M. Baneshi, V. Kiarostami, Optimization and modeling of simultaneous ultrasound-assisted adsorption of ternary dyes using copper oxide nanoparticles immobilized on activated carbon using response surface methodology and artificial neural network, *Ultrason. Sonochem.* 51 (2019) 264–280, <https://doi.org/10.1016/j.ultsonch.2018.10.007>.
- [41] F. Ye, S. Ma, L. Tong, J. Xiao, P. Bénard, R. Chahine, Artificial neural network based optimization for hydrogen purification performance of pressure swing adsorption, *Int. J. Hydrogen Energy* 44 (2019) 5334–5344, <https://doi.org/10.1016/j.ijhydene.2018.08.104>.
- [42] S. Nag, N. Bar, S.K. Das, Sustainable bioremediation of Cd(II) in fixed bed column using green adsorbents: application of Kinetic models and GA-ANN technique, *Environmental Technology & Innovation* 13 (2019) 130–145, <https://doi.org/10.1016/j.eti.2018.11.007>.
- [43] B.G. Saucedo-Delgado, D.A. De Haro-Del Rio, L.M. González-Rodríguez, H.E. Reynel-Ávila, D.I. Mendoza-Castillo, A. Bonilla-Petriciolet, J. Rivera de la Rosa, Fluoride adsorption from aqueous solution using a protonated clinoptilolite and its modeling with artificial neural network-based equations, *J. Fluorine Chem.* 204 (2017) 98–106, <https://doi.org/10.1016/j.jfluchem.2017.11.002>.
- [44] T. Mitra, B. Singha, N. Bar, S.K. Das, Removal of Pb(II) ions from aqueous solution using water hyacinth root by fixed-bed column and ANN modeling, *J. Hazard Mater.* (2014) <https://doi.org/10.1016/j.jhazmat.2014.03.025>.
- [45] D.I. Mendoza-Castillo, H.E. Reynel-Ávila, F.J. Sánchez-Ruiz, R. Trejo-Valencia, J.E. Jaime-Leal, A. Bonilla-Petriciolet, Insights and pitfalls of artificial neural network modeling of competitive multi-metallic adsorption data, *J. Mol. Liq.* 251 (2018) 15–27, <https://doi.org/10.1016/j.molliq.2017.12.030>.
- [46] K. Sharafi, M. Pirsaeheb, V.K. Gupta, S. Agarwal, M. Moradi, Y. Vasseghian, E.-N. Dragoi, Phenol adsorption on scoria stone as adsorbent - application of response surface method and artificial neural networks, *J. Mol. Liq.* 274 (2019) 699–714, <https://doi.org/10.1016/j.molliq.2018.11.006>.
- [47] R.R. Karri, J.N. Sahu, Process optimization and adsorption modeling using activated carbon derived from palm oil kernel shell for Zn (II) disposal from the aqueous environment using differential evolution embedded neural network, *J. Mol. Liq.* 265 (2018) 592–602, <https://doi.org/10.1016/j.molliq.2018.06.040>.
- [48] K.V. Kumar, K. Porkodi, Modelling the solid-liquid adsorption processes using artificial neural networks trained by pseudo second order kinetics, *Chem. Eng. J.* 148 (2009) 20–25, <https://doi.org/10.1016/j.cej.2008.07.026>.
- [49] A. Muthukkumaran, *Analyses of Single and Binary Dye Adsorption Using Simulations and Design of Experiments*, IIT Madras, 2017.
- [50] G.W. Ewing, *Instrumental Methods of Chemical Analysis*, fifth ed. McGraw-Hill, 1985.
- [51] R. Mirzajani, F. Kardani, Fabrication of ciprofloxacin molecular imprinted polymer coating on a stainless steel wire as a selective solid-phase microextraction fiber for sensitive determination of fluoroquinolones in biological fluids and tablet formulation using HPLC-UV detection, *J. Pharm. Biomed. Anal.* (2016) <https://doi.org/10.1016/j.jpba.2016.01.046>.
- [52] Y.-S. Hong, C.-J. Kim, K.-R. Sin, J.-S. Pak, A new adsorption rate equation in batch system, *Chem. Phys. Lett.* 706 (2018) 196–201, <https://doi.org/10.1016/j.cplett.2018.06.010>.